

Interface control and snow crystal growth

Jessica Li ^a and Laura P. Schaposnik ^b

(a) Kent Place School, 42 Norwood Avenue, Summit, NJ 07902, USA

(b) Department of Mathematics, University of Illinois, Urbana, IL 61801, USA

The growth of snow crystals is dependent on the temperature and saturation of the environment. In the case of dendrites, Reiter's local two-dimensional model provides a realistic approach to the study of dendrite growth. In this paper we obtain a new geometric rule that incorporates interface control, a basic mechanism of crystallization that is not taken into account in the original Reiter's model. By defining two new variables, growth latency and growth direction, our improved model gives a realistic model not only for dendrite but also for plate forms.

Keywords:

I. INTRODUCTION

Snowflake growth is a specific example of crystallization - how crystals grow and create complex structures. Because crystallization corresponds to a basic phase transition in physics, and crystals make up the foundation of several major industries, studying snowflake growth helps gaining understanding of how molecules condense to form crystals. This fundamental knowledge may help fabricate novel types of crystalline materials [7].

Whilst current computer modelling methods can generate snowflake images that successfully capture some basic features of real snowflakes, certain fundamental features of snowflakes growth are not well understood. One of the key challenges has been that the snowflake growth models consist of a large set of PDEs, and as in many chaos theoretic problems, rigorous study is difficult.

Snowflakes exhibit a rich combination of characteristic symmetry and complexity. The six fold symmetry is a result of the hexagonal structure of the ice crystal lattice, and the complexity comes from the random motion of individual snow crystals falling through the atmosphere:



FIG. 1: Examples of real plate and dendrite snowflakes [9]. (a) Stellar dendrite (b) Stellar plate (c) Sectorial plate.

Scientific studies of snowflakes can be categorized into two main types. The first approach takes a macroscopic view by observing natural snowflakes in a variety of morphological environments characterized by temperature, pressure and vapour density (see [12–14] and references therein). The second type takes a microscopic view and investigates the basic physical mechanisms governing the growth of snowflakes (e.g. see [7]). While some aspects of snowflake growth (e.g., the crystal structure of ice) are well understood, many other aspects such as diffusion limited growth are at best understood at a qualitative level [7].

Another approach in which snowflake growth is numerically simulated to produce images with mathematical models derived from physical principles is through computer modelling (e.g. see [3, 4, 15–17, 19]). By comparing computer generated images with actual snowflakes, one can correlate the mathematical models and their parameters with physical conditions. While computer modelling can generate snowflake images that successfully capture some basic features of actual snowflakes, so far there has been only limited analysis of these computer models in the literature.

In this paper we analyze snowflake growth simulated by the computer models so as to connect the microscopic and macroscopic views and to further our understanding of snowflake physics. The models that have been considered in the past are in essence chaos theoretic models, which is why they successfully capture the real world phenomena, but prove to be notoriously difficult to analyze rigorously. In this paper we study Reiter's popular model [17] using a combined approach of mathematical analysis and numerical simulation.

After reviewing Reiter's model in Section II, in Section III we divide a snowflake image into main branches and side branches and define two new variables (growth latency and growth direction) to characterize the growth patterns. In Section IV we derive a closed form solution of the main branch growth latency using a one dimensional linear model, and compare it with the simulation results using the hexagonal automata. Then, in Section V we discover a few interesting patterns of the growth latency and direction of side branches. On the basis of the analysis and the principle of surface free energy minimization, in Section VI we enhance Reiter's model and thus obtain realistic results both for dendrites and plate forms. We summarize our contributions and present a few future work directions in Section VII.

II. AN OVERVIEW OF REITER'S MODEL

Reiter's model is a hexagonal automata which can be described as follows. Given a tessellation of the plane into hexagonal cells, each cell z has six nearest neighbours. We shall denote by $s_t(z) \in \mathbb{R}_{>0}$ the state variable of cell z at time t which gives the amount of water stored in z .

Then, cells are divided into three types:

Definition 1 A cell z is frozen if $s_t(z) \geq 1$ (an *F-cell*). If a cell is not frozen itself but at least one of the nearest neighbours is frozen, the cell is a boundary cell (a *B-cell*). A cell that is neither frozen nor boundary is called nonreceptive (an *NR-cell*). The union of frozen and boundary cells are called receptive cells (*R-cells*).

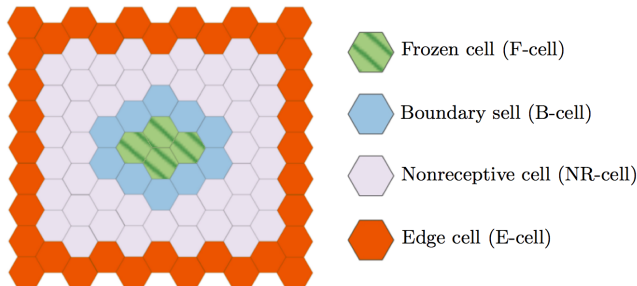


FIG. 2: Classification of cells.

The initial condition in Reiter's model is

$$s_0(z) = \begin{cases} 1 & \text{if } z = \mathcal{O} \\ \beta & \text{if } z \neq \mathcal{O} \end{cases}$$

where \mathcal{O} is the origin cell, and β represents a fixed constant *background vapour level*.

Definition 2 Define the following functions on a cell z : the amount of water that participates in diffusion $u_t(z)$; and the amount of water that does not participate $v_t(z)$. Hence,

$$s_t(z) = u_t(z) + v_t(z) \quad (1)$$

and we let $v_t(z) := s_t(z)$ if z is receptive, and $v_t(z) := 0$ if z is non-receptive.

For γ, α two fixed constants representing *vapour addition* and *diffusion coefficients* respectively, in Reiter's model the state of a cell evolves as a function of the states of its nearest neighbours according to two local update rules that reflect the underlying mathematical models:

- *Constant addition.* For any receptive cell z ,

$$v_t^+(z) := v_t^-(z) + \gamma \quad (2)$$

- *Diffusion.* For any cell z ,

$$u_t^+(z) := u_t^-(z) + \frac{\alpha}{2}(\bar{u}_t^-(z) - u_t^-(z)), \quad (3)$$

where we have used upper indices \pm to denote new functions giving the state variable of a cell before and after a step is completed, and written $\bar{u}_t^-(z)$ for the average of u_t^- for the six nearest neighbours of cell z .

The underlying physical principle of Eq. (3) is the diffusion equation

$$\partial u / \partial t = a \nabla^2 u, \quad (4)$$

where a is a constant. Indeed, Eq. (3) is the discrete version of Eq. (4) on the hexagonal lattice, and it states that a cell z retains $(1 - \alpha/2)$ fraction of $u_t^-(z)$, uniformly distributes the remaining to its six neighbours, and receives $\alpha/12$ fraction from each neighbour. The total amount of $u_t(z)$ would be conserved within the entire system, except that a real world simulation consists of a finite number of contiguous cells. The cells at the edge of the simulation setup are referred to as *edge cells*, in which one sets $u_t^+(z) := \beta$. Thus, water is added to the system via the edge cells in the diffusion process. Combining the two intermediate variables, one obtains

$$s_{t+1}(z) := u_t^+(z) + v_t^+(z). \quad (5)$$

By varying the parameters α, β, γ in Reiter's model one can generate certain geometric forms of snowflakes observed in nature:

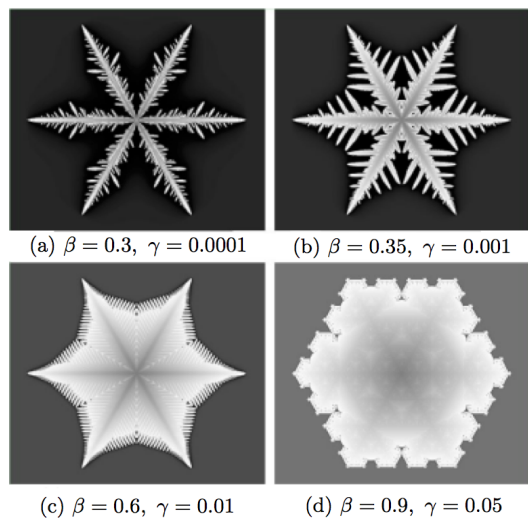


FIG. 3: Images generated by Reiter's model [17] for $\alpha = 1$.

III. GENERAL GEOMETRIC PROPERTIES

In what follows, we give new descriptions of snowflake growth and analyze them with a combined approach of mathematical analysis and numerical simulation by considering a coordinate system of cells as in Figure 4(a) below. A cell z is represented by its coordinate (i, j) , for $i, j \in \mathbb{Z}$, with the origin $\mathcal{O} = (0, 0)$. Since there is a six fold symmetry, we only focus on one twelfth of the cells, marked as dark dots, for which $j \geq i \geq 0$:

The images in Figure 3 show that a crystal consists of six main branches that grow along the lattice axes, and numerous side branches that grow from the main branches in a seemingly random manner. The main and side branches exhibit a rich combination of characteristic symmetry and complexity which we shells rudly through the rate of water accumulation of a cell z , defined by

$$\Delta s_t(z) = s_{t+1}(z) - s_t(z).$$

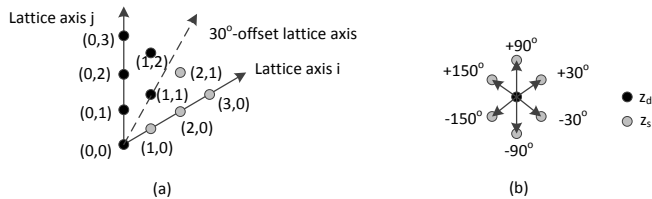


FIG. 4: (a) Coordinate system of hexagonal cells. (b) Definition of growth directions in the coordinate system

At any time the set of all the R-cells is connected. Moreover since a frozen cell is surrounded by receptive cells and does not accumulate water via diffusion, and since water flows from nonreceptive cells to boundary cells, one has that the rate of water accumulation $\Delta s_t(z)$ of a cell satisfies the following general geometric properties:

- (A) For an NR-cell z , one has $0 < s_t(z) \leq \beta$ and $\Delta s_t(z) \leq 0$. Suppose that an NR-cell z is surrounded by R-cells and disconnected from the E-cells. If $\gamma > 0$, there exists $t_0 > 0$ such that $s_{t_0}(z) \geq 1$ (i.e., a time t_0 in which the cell becomes frozen); otherwise, the NR-cell will permanently remain non-receptive and never become frozen.
- (B) For a B-cell z the quantity $\Delta s_t(z)$ is the sum of γ and diffusion. If $\gamma > 0$, there exists $t_0 > 0$ such that $s_{t_0}(z) \geq 1$; otherwise, if cell z is surrounded by a set of F-cells and disconnected from the E-cells, then as in (A), the cell will never become frozen:

$$\lim_{t \rightarrow \infty} s_t(z) < 1.$$

- (C) For an F-cell z , one has $\Delta s_t(z) = \gamma$.
- (D) The state variable of a cell is $s_t(z) = \beta$ only for z an E-cell.

Thus, for an NR-cell to become frozen, the cell goes through two stages of growth. First, the NR-cell loses vapour to other cells due to diffusion, as in (A). Subsequently, it becomes a B-cell and accumulates water via diffusion and addition, as in (B), until it becomes frozen and sees no benefit of diffusion, as in (C). Becoming a B-cell is a critical event between the two stages.

We focus on the second stage and define two new variables to characterize growth patterns.

Definition 3 *The time to be frozen of a cell z is denoted by $T(z)$ and defined by the condition $s_{T(z)}(z) \geq 1$, and $s_t(z) < 1$ for $t < T(z)$. Similarly, we define $B(z)$ as the first time to be boundary. Finally, growth latency is denoted by $L(z)$ and defined by $L(z) := T(z) - B(z)$.*

A cell becomes a B-cell as one of its neighbouring cells has just become an F-cell, and thus it is useful to make the following definition in terms of redistribution of water:

Definition 4 *Denote by z_d a destination cell, and by z_s a source cell. Then, the growth direction of cell z_d is denoted by $g(z_d)$ and defined as the orientation of z_s with respect to z_d , where the angle is with respect to the horizontal axis. The source-destination cell relationship shall be denoted by $S(z_d) := z_s$.*

As shown in Figure 4(b), the angle is given relative to the horizontal direction in the coordinate system, and satisfies

$$g(z_d) \in \{+30^\circ, -30^\circ, +90^\circ, -90^\circ, +150^\circ, -150^\circ\}.$$

Note that while the growth of z_d is traced back to a unique z_s , a source cell may correspond to multiple destination cells.

IV. GROWTH OF MAIN BRANCHES

Consider cells (i, j) where $i + j = K$ for a fixed K . These cells are all K sites away from the origin $(0, 0)$ on the grid. The main branch growth pattern is such that $T(0, K) \leq T(i, j)$ and

$$\begin{aligned} T\left(\frac{K}{2}, \frac{K}{2}\right) &\geq T(i, j) \quad \text{for even } K, \\ T\left(\frac{K-1}{2}, \frac{K-1}{2}\right) &\geq T(i, j) \quad \text{for odd } K. \end{aligned}$$

Along the lattice j -axis, one has $g(0, j) = -90^\circ$ for all j . Hence, the snowflake growth is fastest along a lattice axis, which represents a main branch, and is the slowest along the 30°-offset lattice axis.

We next develop a model to calculate the growth latency $L(0, j)$. As cell $(0, j)$ becomes frozen, cell $(0, j+1)$ becomes a boundary cell. Hence the first time to be boundary $B(0, j+1) = T(0, j)$, and thus one can calculate $T(0, j)$ as

$$T(0, j) = T(0, 0) + \sum_{k=1}^j L(0, k). \quad (6)$$

In order to gain analytical understanding, we first study a one dimensional model. Consider a line of consecutive cells z_0, z_1, \dots, z_N , where z_N is the edge cell. Initially cell \mathcal{O} is frozen. We focus on the growth period $[B(k), T(k)]$ in which cells z_0, z_1, \dots, z_{k-1} are frozen and cell k grows from boundary to frozen. Since Eq. (3) describes the diffusion dynamics of vapour being transferred from the edge cell to cell z_k , and cell z_k accumulates water via addition Eq. (2), to derive an analytical solution, we make the following assumption which we justify shortly.

Assumption 1 *For $t \in [B(z_k), T(z_k)]$, assume that in Eq. (3) one has*

$$u_t^+(z_i) = u_t^-(z_i),$$

for $k+1 \leq i \leq N$, for N as above and $B(z_k), T(z_k)$ as in Definition 3. Therefore, the vapour distribution reaches a steady state, denoted as $\mu(i|k)$.

From Assumption 1, we can ignore the notations of \pm , and reduce Eq. (3) to the linear equation

$$\mu(i|k) = \frac{1}{2} \left(\mu(i-1|k) + \mu(i+1|k) \right). \quad (7)$$

Moreover, with the boundary conditions $\mu(k|k) = 0$ and $\mu(N|k) = \beta$, the vapour distribution can be written in a closed form as follows:

$$\mu(i|k) = \frac{i-k}{N-k} \beta, \text{ for } i = k, \dots, N, \quad (8)$$

which graphically represents a line that connects the two boundary condition points.

We shall now explain why Assumption 1 is well motivated. Suppose that the steady state distribution Eq. (8) is already reached at $t = B(z_k)$, this is,

$$s_{B(z_k)}(z_i) = \mu(i|k-1) = \frac{i-(k-1)}{N-(k-1)} \beta \text{ for } i = k, \dots, N.$$

Then, $s_t(z_i)$ evolves in the interval of $(B(z_k), T(z_k)]$ in the following manner. For $N \gg k$, one has

$$s_{B(z_k)}(z_k) = \mu(k|k-1) = \frac{1}{(N-k+1)} \beta \approx 0.$$

Thus it is reasonable to assume

$$L(z_k) = T(z_k) - B(z_k) \gg 1$$

because cell z_k will take several simulation steps to reach $s_{T(z_k)}(z_k) \geq 1$. Moreover,

$$|s_{B(z_k)}(z_i) - \mu(i|k)| = \left| \frac{i-(k-1)}{N-(k-1)} \beta - \frac{(i-k)}{(N-k)} \beta \right| \ll 1$$

for $N \gg k$. Thus, in each simulation step for time $t \in (B(z_k), T(z_k)]$, the function $s_t(z_i)$ only varies slightly and can be considered approximately constant. Hence, $u_t^+(z_i) = u_t^-(z_i)$.

From Eq. (3) and Eq. (7), we may estimate $u_t^+(z_k)$ by

$$\hat{u}_t^+(z_k) := \frac{\alpha}{4} \frac{1}{N-k} \beta.$$

Moreover, since $u_t^-(z_k) = 0$ it follows that we can further estimate $\Delta s_t(z_k)$ and $L(z_k)$ by

$$\Delta \hat{s}_t(z_k) := \frac{\alpha}{4} \frac{1}{N-k} \beta + \gamma, \quad (9)$$

$$\hat{L}(z_k) := \frac{1 - s_{B(z_k)}(z_k)}{\Delta \hat{s}_t(z_k)} = \frac{1 - \frac{1}{N-k+1} \beta}{\frac{\alpha}{4} \frac{1}{N-k} \beta + \gamma}. \quad (10)$$

In the one dimensional model with $N = 50$, we may compare the vapour accumulation in every simulation step, as the simulation proceeds from the time when cell $k = 25$ just becomes boundary to the time when it becomes frozen. Figure 5 compares $\Delta s_t(z_k)$ at cell z_k determined by the simulation, and $\Delta \hat{s}_t(z_k)$ predicted by Eq. (9) for time $t \in [B(z_k), T(z_k)]$. Initially $s_t(k) \ll \mu(i|k)$, and $\Delta s_t(k) \gg \Delta \hat{s}_t(k)$. After about 5 simulation steps, $\Delta s_t(k)$ drops to a flat plateau, which is approximately equal to $s_t(k)$. At any time t , one observes that $\Delta \hat{s}_t(k) \leq \Delta s_t(k)$.

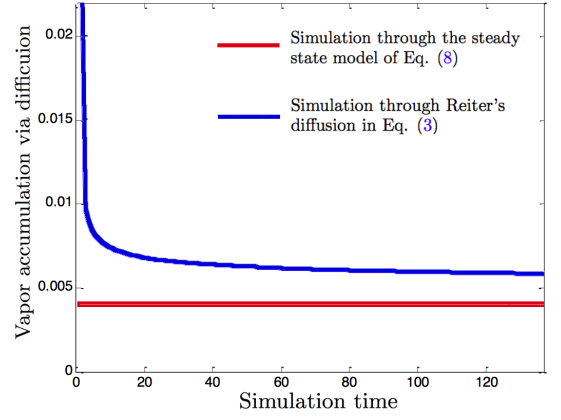


FIG. 5: Comparison of vapour accumulation simulations for the parameters $\alpha = 1$, $\beta = 0.4$, $\gamma = 0.001$.

One may also model $L(z_k) = T(z_k) - B(z_k)$ as a function of cell index of the cells. In the one dimensional model with $N = 50$, Figure 6 compares $L(k)$ determined by the simulation, and $\hat{L}(z_k)$ predicted by Eq. (10) as the snowflake grows from the origin \mathcal{O} to the edge cell. For any k , one observes that $L(z_k) < \hat{L}(z_k)$. This phenomenon is expected, since by solving the above PDE's one has that there exists $\alpha > 0$ such that at any time instance $t \in [B(z_k), T(z_k)]$, for $i = k, \dots, N$, one has

$$\mu(i|k) \leq s_t(z_i) \text{ and } \Delta \hat{s}_t(z_k) \leq \Delta s_t(z_k).$$

As a result, $\hat{L}(z_k) \geq L(z_k)$.

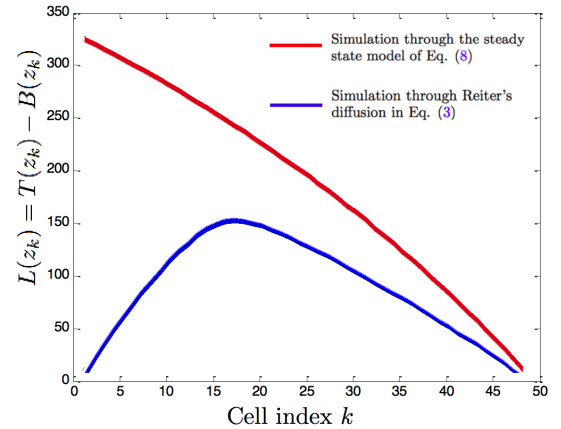


FIG. 6: Comparison of growth latency simulations for the parameters $\alpha = 1$, $\beta = 0.4$, $\gamma = 0.001$.

Equation Eq. (10) predicts that $\hat{L}(z_k)$ drops monotonically with k . In simulation, we observe that in the beginning the cells grow from boundary to frozen very quickly, well before the steady state is reached. As a result, the steady state Assumption 1 does not hold in that time period. Figure 6 shows that $L(z_k)$ first increases, then drops, and eventually matches the prediction $\hat{L}(z_k)$.

Finally, we return to the two dimensional hexagonal cellular case. With a similar steady state assumption, we can reduce the PDE to a set of linear equations similar to Eq. (7). However, the geometric structure is much more

complex than the one dimensional case. As a result, it is difficult to derive a closed form formula of the vapour distribution similar to Eq. (8).

Figure 7 below plots $L(0, j)$ along a main branch. Comparison with Figure 6 indicates a similarity between the one dimensional and two dimensional cases in that $L(z)$ increases as the snowflake grows from the origin. However, in the two dimensional case, we observe from simulations that $L(0, 10) = L(0, 11) = \dots = L(0, 195)$. When the snowflake grows close to the edge cell, it experiences some edge effect in the simulation where L drops drastically. This indicates that somewhat surprisingly $\Delta s_t(0, j)$ remains almost constant as the snowflake grows along the main branch.

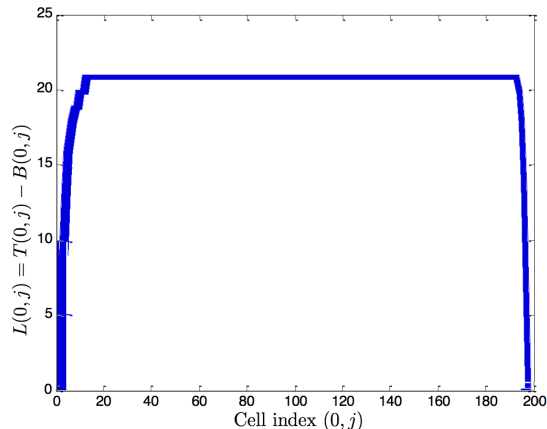


FIG. 7: $T(0, j) - B(0, j)$ of cells $(0, j)$ along a main branch for $j = 1, 2, \dots$, in the two dimensional scenario. Here cell $(0, 200)$ is an edge cell, and $\alpha = 1$, $\beta = 0.4$, $\gamma = 0.001$.

V. GROWTH OF SIDE BRANCHES

While the main branches of snowflakes represent clean six fold symmetry, the side branches exhibit characteristic features of chaotic dynamics: complexity and unpredictability. Reiter's model is completely deterministic with no noise or randomness involved, and yet the resultant snowflake images are sensitive to the parameters α, β , and γ in a chaotic manner. Chaos may appear to be the antithesis of symmetry and structure. Our goal in this section is to discover growth patterns that emerge from seemingly chaotic dynamics.

Definition 5 Starting from a cell z_0 on the j -axis main branch, the set of consecutive frozen cells in the i -axis direction are referred to as side branch from cell z_0 . We shall denote by $z_E(z_0)$ the outmost cell or tip, by $E(z_0)$ the length of the side branch, and the side branch itself by $\Phi(z_0) := \{z_0, \dots, z_E(z_0)\}$.

In what follows, we study the growth latency of side branches. Figure 8 below plots the tips of the side branches that grow from the j -axis main branch using the parameters of the four images in Figure 3.

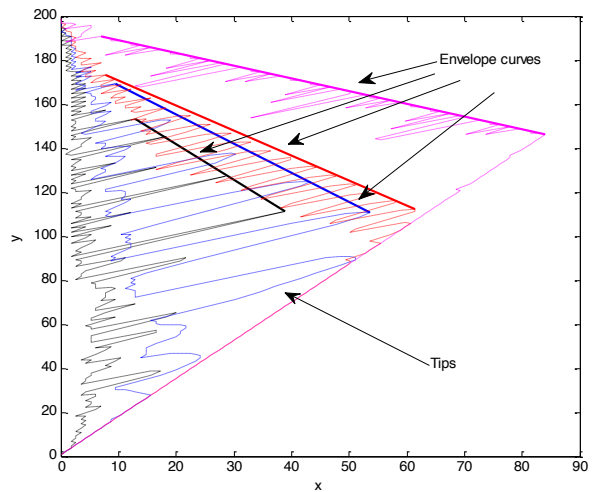


FIG. 8: Plots of the tips (thin curves) and envelope curves (thick curves) of the side branches from the j -axis main branch using the parameters of the four example images in Figure 3. Due to symmetry, we focus on one set of side branches that grow from the right side of lattice j -axis. Here, the black curve represents Figure 3(a), blue for Figure 3(b), red for Figure 3(c), and magenta for Figure 3(d). The axes here are the horizontal and vertical axes of the coordinate system.

Due to the chaotic dynamics, the lengths of the side branches vary drastically with z_0 in a seemingly random manner. For image (a), most of the side branches are short and only a small number stand out. The opposite holds for image (d). The scenarios are in between for images (b) and (c). The length of the side branches is indicative of the growth latency. The long side branches represent the ones that grow fastest. In Figure 8 we connect the tips of the long side branches to form an *envelope curve* that represents the frontier of the side branch growth. The most interesting observation is that the envelope curve can be closely approximated by a straight line for the most part. Recall that the growth latency of the main branch is a constant. Thus we infer that the growth latency of the long side branches is also constant. Denoting by L_M and L_S the *growth latencies* of the main and long side branches respectively, one has that

$$\frac{L_M}{L_S} = \frac{\sin 2\pi/3 - \theta}{\sin \theta} \quad (11)$$

where θ is the angle between the envelope curve straight line and the j -axis. As a specific example, for the magenta curve, the envelope curve of the long side branches grows almost as fast as the main branch, such that $\theta \approx \pi/3$ and the resultant image, appearing in Figure 3(d), is roughly a hexagon.

We shall consider next the growth directions of the cells on side branches. Figure 9 below plots the trace of the growth direction $g(z)$ (see Definition 4) as a snowflake develops in the simulation. The corresponding snowflake image is shown in Figure 3(b). When a cell z becomes

boundary, we mark the cell to indicate $g(z)$ using the legend labeled in the figure. If a cell never becomes boundary, no mark is made. All side branches grow from the j -axis main branch, starting in the direction parallel to the i -axis. Subsequently, a side branch may split into multiple directions. Indeed, all six orientations have been observed and the dynamics appear chaotic as $g(z)$ appears unpredictable. However, we do find an interesting pattern described below.

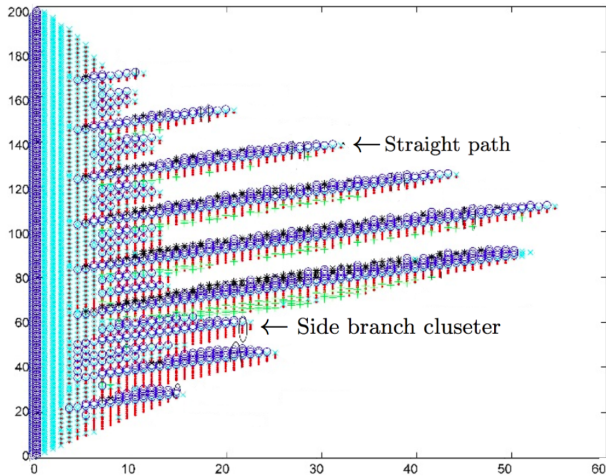


FIG. 9: Trace of relative orientations of source cells with respective destination cells. A destination cell becomes boundary because a source cell, which is one of the neighbours of the destination cell, becomes frozen. Legend is as follows: magenta \blacksquare : $+30^\circ$, black \star : -30° , green $+$: $+90^\circ$, blue \circ : -90° , red \cdot : $+150^\circ$, cyan \times : -150° , where the parameters are $\alpha = 1$, $\beta = 0.35$, $\gamma = 0.001$. Note that not all straight paths are labeled. The axis are as in Figure 4(a).

Definition 6 A straight path from a cell z_0 on the j -axis main branch is the set of consecutive frozen cells in the i -axis direction satisfying $z_{i-1} = S(z_i)$. The number of consecutive cells satisfying $z_{i-1} = S(z_i)$ is the length $F(z_0)$. We then denote a straight path from a cell z_0 by $\Psi(z_0) := \{z_0, z_1, z_2, \dots, z_{F(z_0)}\}$.

Comparison between Definition 5 and Definition 6 shows that the paths are nested, i.e. $\Psi(z_0) \subset \Phi(z_0)$, and hence the lengths satisfy $F(z_0) \leq E(z_0)$. When a cell z_{i-1} on the straight path becomes frozen, it triggers not only z_i in the i -axis direction but also other neighbours to become boundary, resulting in growth in other directions, which we call *deviating paths*. The straight and deviating paths collectively form a *side branch cluster*.

Definition 7 The set of frozen cells that can be traced back to a cell on the straight path from cell z_0 on the j -axis main branch is referred to as a side branch cluster and denoted by $\Theta(z_0)$.

A side branch cluster is a visual notion of a collection of side branches that appear to grow together. Figure 9 shows several side branch clusters and the cells on the corresponding straight path marked with cyan \times .

Compared with the straight paths, the deviating paths do not grow very far, because they compete with other straight or deviating paths for vapour accumulation in diffusion. On the other hand, the competition with the deviating paths slows down or may even block the growth of a straight path. When a straight path is blocked, the straight path is a strict subset of the corresponding side branch. This scenario is illustrated in Figure 10, where three side branches are shown.

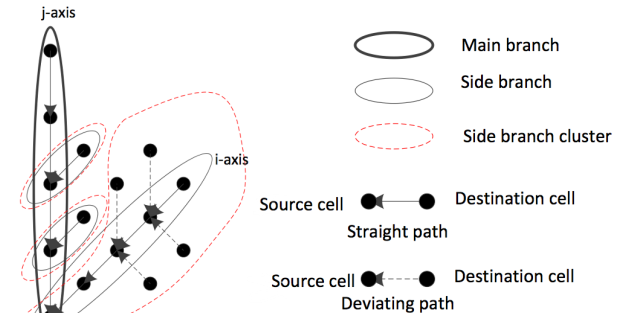


FIG. 10: An arrow linking two cells indicates the source/destination relationship.

The straight path of the middle side branch is blocked by a deviating path of the lower side branch, which grows into a sizeable side branch cluster. Through the above definitions one has that if there exists a cell z such that $z \in \Theta(z_0)$ and $z \notin \Phi(z'_0)$, then the paths are nested $\Psi(z'_0) \subset \Phi(z'_0)$. Moreover, the straight path determines the length of the side branch cluster:

Definition 8 Denote by $D(z, z_0)$ the distance between $z, z \in \Theta(z_0)$, defined as the smallest number of sites on the lattice between z and z_0 . The length of $\Theta(z_0)$ is

$$D(z_0) := \max_{z \in \Theta(z_0)} D(z, z_0).$$

Through the above definition one can show that there are K cells $z_i \in \Theta(z_0)$ such that the distances satisfy $D(z_i, z_0) = D(z_0)$ for $i = 1, \dots, K$ with $K \geq 2$. Furthermore, there exists $z_i \in \Psi(z_0)$ for $1 \leq i \leq K$, and thus $D(z_0) = F(z_0)$, the length of $\Psi(z_0)$ as in Definition 6.

VI. AN ENHANCED REITER'S MODEL

Plates and dendrites are two basic types of regular, symmetrical snowflakes. We observe that while the dendrite images in Figure 3(a)(b) generated by Reiter's model resemble quite accurately the real snowflake in Figure 1(a), as seen in Figure 3(c)(d) and Figure 1(b)(c), the plate images differ significantly. The plate images in Figure 3(c)(d) is in effect generated as a very leafy dendrite. One of the reasons that Reiter's model is unable to generate plate images realistically is that the model only includes diffusion, thus not taking into account the effect of local geometry.

As described in [1], two basic types of mechanisms contribute to the solidification process of snowflakes: diffusion control and interface control. Diffusion control is a non geometric growth model, where snowflake surfaces are everywhere rough due to diffusion instability, a characteristic result of chaotic dynamics. For example, if a plane snowflake surface develops a small bump, it will have more exposure into the surrounding vapour and grow faster than its immediate neighbourhood due to diffusion. Interface control is a geometric mechanism where snowflake growth only depends on local geometry, i.e., curvature related forces. In the small bump example, the surface molecules on the bump with positive curvature have fewer nearest neighbours than do those on a plane surface and are thus more likely to be removed, making the bump move back to the plane. Interface control makes snowflake surfaces smooth and stable, and it is illustrated in Figure 11 below.

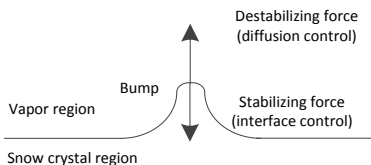


FIG. 11: Two competing forces of diffusion control and interface control that determine snowflake growth.

In summary, snowflake growth is determined by the competition of the destabilizing force (diffusion control) and stabilizing force (interface control). In the absence of interface control, Reiter’s model is unable to simulate certain features of snowflake growth.

The interface between the snowflake and vapour regions has potential energy, called surface free energy, due to the unfilled electron orbitals of the surface molecules. The *surface free energy* $\gamma(n)$ as a function of direction n , is determined by the internal structure of the snowflake, and in the case of a lattice plane, is proportional to lattice spacing in a given direction. Figure 12 below plots the surface free energy $\gamma(n)$ of a snowflake as a function of the direction n .

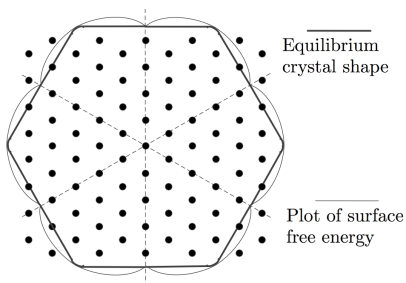


FIG. 12: Surface free energy of snowflake as a function of direction and equilibrium crystal shape of snowflake derived from surface free energy plot with Wulff construction [1].

The equilibrium shape of the interface is the one that minimizes the total surface free energy for a given enclosed volume. Wulff construction (see [1]) can be used

to derive the equilibrium crystal shape \mathcal{W}_γ from the surface free energy plot $\gamma(n)$:

$$\mathcal{W}_\gamma := \{r \mid r \cdot n \leq \gamma(n), \forall n\}. \quad (12)$$

Wulff construction states that the distances of the equilibrium crystal shape from the origin are proportional to their surface free energies per unit area. Figure 12 plots the equilibrium crystal shape of snowflake. Moreover, it shows that due to interface control, snowflake growth is the slowest along the lattice axes, and the fastest along the 30° -offset lattice axes.

This can be explained intuitively. Snowflake grows by adding layers of molecules to the existing surfaces. The larger the spaces between parallel lattice planes, the faster the growth is in that direction. This effect is completely opposite to the diffusion control we have studied in Section 4, where snowflake grows fastest along the lattice axes. This is an example of competition between diffusion control and interface control.

We next propose a new geometric rule to incorporate interface control in Reiter’s model. The idea is that the surface free energy minimization forces the lattice points on an equilibrium crystal shape to possess the same amount of vapour so that the surface tends to converge to the equilibrium crystal shape as the snowflake grows.

From Figure 12, we learn that the equilibrium crystal shape is a hexagon except for six narrow regions along the 30° -offset lattice axes where the transition from one edge of the hexagon to another edge is smoothed. The equilibrium crystal shape used in the new geometric rule is shown in Figure 13.

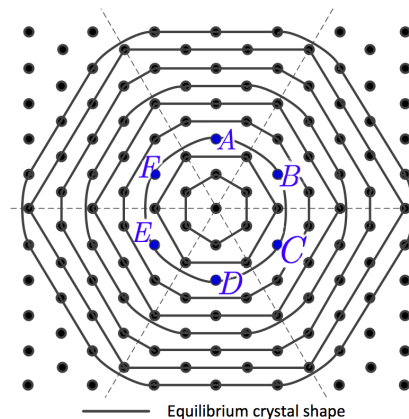


FIG. 13: Equilibrium crystal shape used in the new geometric rule.

Figure 13 shows the equilibrium crystal shape used in the new geometric rule and the interface control neighbours of the cells. As an example, cells A, B, C, D, E, F are on the same equilibrium crystal shape. Cells F, B are the interface control neighbours of A , cells A, C are the interface control neighbours of B , etc.

The new geometric rule is applied after Eq. (5): a new variable $\delta_t(z)$ is defined to represent the *amount of water to be redistributed for cell z at time t* , with initial value $\delta_t(z) = 0$ for all z .

Definition 9 For a given cell z_0 , define two interface control neighbours z_0^1, z_0^2 , which are two neighbouring cells of z_0 on the same equilibrium crystal shape.

Define $\bar{s}(z_0)$ as the average of the water amounts in cell z_0 and its two interface control neighbours z_0^1, z_0^2 , this is:

$$\bar{s}(z_0) := \frac{1}{3} \left(s_{t+1}^-(z_0) + s_{t+1}^-(z_0^1) + s_{t+1}^-(z_0^2) \right). \quad (13)$$

For every boundary z_0 , if neither of z_0^1, z_0^2 are frozen, then adjust $\delta_t(z_0)$ as follows

$$\delta_s(z_0) = \delta_s(z_0) + \varepsilon(\bar{s}(z_0) - s_{t+1}^-(z_0)), \quad (14)$$

$$\delta_s(z_0^1) = \delta_s(z_0^1) + \varepsilon(\bar{s}(z_0) - s_{t+1}^-(z_0^1)), \quad (15)$$

$$\delta_s(z_0^2) = \delta_s(z_0^2) + \varepsilon(\bar{s}(z_0) - s_{t+1}^-(z_0^2)), \quad (16)$$

where $\varepsilon \in \mathbb{R}_{\geq 0}$ determines the amount of interface control. After $\delta_s(z)$ has been adjusted for all z according to Eq. (14)-(16), for every cell z set

$$s_{t+1}^+(z) := s_{t+1}^-(z) + \delta_s(z). \quad (17)$$

Recall that in the original Reiter's model, once water is accumulated in a boundary cell, water stays permanently in that cell. The new function Eq. (17) forces water redistribution particularly among boundary cells to smoothen the snow vapour interface. Figure 14 below shows two snowflake images generated by the enhanced Reiter's model with the new geometric rule.

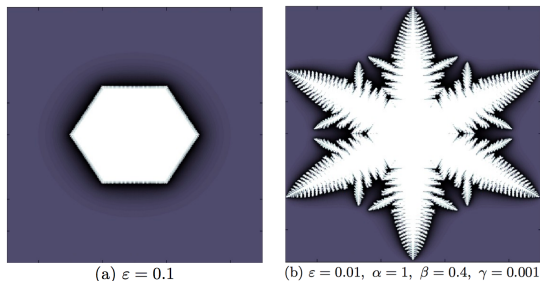


FIG. 14: Snowflake images generated by the enhanced Reiter's model with the new geometric rule.

At $\varepsilon = 0.1$, the image above resembles a plate observed in nature much more closely than the ones in Figure 3. By reducing interface control with $\varepsilon = 0.01$, the snowflake starts as a plate and later becomes a dendrite as diffusion control dominates interface control.

VII. CONCLUSIONS AND FUTURE WORK

In this paper we have analyzed the growth of snowflake images generated by a computer simulation model (Reiter's model [17]), and have proposed ways to improve the model. We have derived an analytical solution of the main branch growth latency and made numerical comparison with simulation results. Subsequently we observed interesting patterns of side branches in terms of

growth latency and direction. Finally, to enhance the model, we have introduced a new geometric rule that incorporates interface control, a basic mechanism of the solidification process, which is not present in the original Reiter's model.

The present work has shed light into some interesting patterns that lead to further questions about crystal growth. On the main branch growth, one may ask why the growth latency is almost constant (Figure 7) and whether this phenomenon is unique to the hexagonal cells or applicable to other two dimensional lattices. Concerning the side branch growth, it was noted that some side branches grow much faster than their neighbours, and that with slightly different diffusion parameters the side branch growth latency could change drastically at the same position while the main branch growth latency remains virtually the same. The study in Section VI shows that this great sensitivity is attributable to diffusion instability - when the growth of cells in some direction gain initial advantage over their neighbours, the advantage continues to expand such that the growth in that direction becomes even faster. It was noted in Section VI that diffusion instability is caused by competition among cells in diffusion, and thus the average number of contributing neighbours is a good indicator to explain diffusion instability. Finally, the enhanced model described in Section VI can be used to explore the interplay of diffusion and interface control. For example, one may simulate growth in an environment where the diffusion and interface control parameters vary with time so as to generate images similar to Figure 1 (b)(c).

Recently Reiter's model was used in the study of snowfall retrieval algorithms (e.g. see [6, 18] and references therein), and it was suggested that other mechanisms of snowflake formation from ice crystals besides aggregation must be considered in snowfall retrieval algorithms. It is thus natural to ask whether the enhanced Reiter's model constructed here may provide novel insights in this direction, as well as when considering crystal growth dynamics as in [8]. Moreover, since cellular automata models have been considered for numerical computations of pattern formation in snow crystal growth, it would be interesting to analyze the outcome of the implementation of the model presented here to the analysis done in [2, 5].

Finally, the effects of lattice anisotropy coupled to a diffusion process have been studied in [10] to understand phase diagrams associated to crystal growth. Since this approach seemed recently useful from different perspectives (e.g. see [11] and references therein), it would be interesting to study the enhanced model constructed here from the perspective of [10, 11].

Acknowledgments: The research in this paper was conducted by the first author under the supervision of the latter, as part of the IGL & MIT-PRIMES program. Both authors are thankful for the opportunity to conduct this research together, and would also like to thank K. Libbrecht and N. Goldenfeld for helpful comments.

-
- [1] J.A. Adam, *Flowers of ice beauty, symmetry, and complexity: A review of the snowflake: Winter's secret beauty*. Notices Amer. Math. Soc, 52:402 - 416, 2005.
- [2] J.W. Barrett, H. Garcke, R. Nürnberg, *Numerical computations of faceted pattern formation in snow crystal growth*, Phys. Rev. E 86, 011604 (2012)
- [3] J. Gravner, D. Griffeath, *Modeling snowflake growth II: A mesoscopic lattice map with plausible dynamics*. Physics D: Nonlinear Phenomena, 237(3): 385 - 404, 2008.
- [4] J.Gravner, D.Griffeath, *Modeling snowflake growth III: A three-dimensional mesoscopic approach*. Phys. Rev. E, 79:011601, 2009.
- [5] J.G. Kelly, E.C. Boyer, *Physical improvements to a mesoscopic cellular automaton model for three-dimensional snow crystal growth*, ArXiv:1308.4910 (2013).
- [6] J. Leinonen, D. Moisseev, *What do triple-frequency radar signatures reveal about aggregate snowflakes?*, Journal of Geophysical Research: Atmospheres (2015) 1201, p.p. 229 -239 ISSN:2169-897X
- [7] K.G. Libbrecht, *The physics of snowflakes*. Rep. Prog. Phys., 68:855 - 895, 2005.
- [8] K.G. Libbrecht, *Quantitative modeling of faceted ice crystal growth from water vapor using cellular automata*. Journal of Computational Methods in Physics (2013).
- [9] K.G. Libbrecht, *A guide to snowflakes*. www.its.caltech.edu/~atomic, 2014.
- [10] F. Liu and N.D. Goldenfeld, *Generic features of late stage crystal growth*. Phys. Rev. A 42, 895-903 (1990).
- [11] X. Liu, Y. Pu, P. Wang, Z. Dong, Z. Sun, Y. Hu, *Materials Letters Volume 128*, 263-266, 2014
- [12] C. Magono, C.W. Lee, *Meteorological classification of natural snowflakes*. Journal of the Faculty of Science, Hokkaido University, 1966.
- [13] B. Mason, *The Physics of Clouds*. Oxford University Press, 1971.
- [14] U. Nakaya, *Snowflakes: Natural and Artificial*. Harvard University Press, 1954.
- [15] C. Ning, C. Reiter, *A cellular model for 3-dimensional snowflakelization*. Computers and Graphics, 31:668 - 677, 2007.
- [16] N.H. Packard, *Lattice models for solidification and aggregation*. Institute for Advanced Study preprint, 1984. Reprinted in Theory and Application of Cellular Automata, S. Wolfram, editor, World Scientific, 1986, 305 - 310.
- [17] C. Reiter, *A local cellular model for snowflake growth*. Chaos, Solitons & Fractals, 23:1111 - 1119, 2005.
- [18] J. Tyynelä, V. Chandrasekar, *Characterizing falling snow using multifrequency dual-polarization measurements*, Journal of Geophysical Research: Atmospheres (2014) 119 13 p.p. 8268 -8283 ISSN:2169-897X
- [19] T. Wittern, L. Sander, *Diffusion-limited aggregation, a kinetic critical phenomenon*. Phys. Rev. Lett., 47:1400 - 1403, 1981.